Received: 8 September 2021 | Accepted: 15 April 2022

DOI: 10.1111/2041-210X.13898

Methods in Ecology and Evolution BRITISH ECOLOGICAL SOCIETY

RESEARCH ARTICLE

# Long-term automated visual monitoring of Antarctic benthic fauna

Simone Marini[1,2] | Federico Bonofiglio[1] | Lorenzo P. Corgnati[1] | Andrea Bordone[3] | Stefano Schiaparelli[4,5] | Andrea Peirano[3]

[1]National Research Council of Italy (CNR), Institute of Marine Sciences, La Spezia, Italy

[2]Stazione Zoologica Anton Dohrn, Naples, Italy

[3]ENEA-Marine Environment Research Centre, La Spezia, Italy

[4]DISTAV, Università di Genova, Genova, Italy

[5]5 MNA, Italian National Antarctic Museum (Section of Genoa), Genoa, Italy

**Correspondence**
Simone Marini
Email: simone.marini@sp.ismar.cnr.it

**Handling Editor:** Aaron Ellison

## Abstract

1. The rapid changes in the climate of Antarctica are likely to pose challenges to living communities, which makes monitoring of Antarctic fauna an urgent necessity. Benthos is particularly difficult to monitor, and is sensitive to local environmental changes. At the same time, long-term monitoring is complicated by logistical factors. It is therefore urgent to develop advanced instruments to set up autonomous and long-term monitoring programmes to obtain the lacking biological knowledge needed to understand this complex and remote marine environment.
2. We present a pilot study to set up a non-invasive and sustainable autonomous monitoring activity in Antarctica, leveraging on a specifically designed automated camera recording, computer vision and machine learning image processing techniques. We also present and analyse the high-resolution image dataset acquired for an extended period of time encompassing both the summer and the Antarctic night and the corresponding transition periods.
3. The results of this study demonstrate both the effectiveness of such an autonomous imaging devices for acquiring relevant long-term visual data and the effectiveness of the proposed image analysis algorithms for extracting relevant scientific knowledge from such data. The presented results show how the extracted knowledge discloses dynamics of the observed ecosystems that can be obtained only through continuous observations extended in time, not achievable with the state-of-the-art monitoring approaches commonly implemented in Antarctica.
4. The success of this pilot study is a step towards the collection of continuous data near shore in Antarctic areas and in general in all the remote and extreme underwater habitats. Moreover, the presented stand-alone and autonomous imaging device can be used for increasing the number of the monitoring sites in remote environments and when complemented with the acquisition of physical

and bio-chemical variables it can be used for obtaining data collections of great scientific value difficult to acquire otherwise.

KEYWORDS
Antarctica, artificial intelligence, autonomous imaging device, autonomous marine observing systems, benthic fauna, computer vision, long-term monitoring, underwater images

## 1 | INTRODUCTION

The Southern Ocean and Antarctic coastal seas cover approximately 10% of the area of the world's oceans (Rogers et al., 2020), and only 2.1% of the Antarctica shelf is shallower than 200 m (Peck, 2018). In the recent past, the continent and its surrounding ocean and islands have been the focus of studies in ecology, biology and oceanography (Brasier et al., 2019; Clark et al., 2019; Malyarenko et al., 2020), showing that it is a complex environment where biological, chemical and physical parameters operate either synergistically, additively or antagonistically, and have a significant impact on the coastal environment (Convey & Peck, 2019).

The relatively high level of marine biodiversity in the Southern Ocean depends on an environmental heterogeneity from small to large spatial scales. Such heterogeneity involves variation in latitude, nutrient dynamics and light availability between the austral day and night, but also depends on the variations in the thickness of the covering ice pack and on the scouring effects of icebergs (Barnes, 2017; Rogers et al., 2020).

Anthropic-driven climate change is responsible for the modification of the physical conditions and of the structure of the ecosystem in the Southern Ocean (Rogers et al., 2020). These changes affect the benthic coastal communities mainly as a consequence of an increase in the water temperature, the melting of the ice shelf and the glacial retreat (Rogers et al., 2020). To understand the effect of these environmental changes on the marine Antarctic biodiversity, it is important to understand the functioning of the benthic communities, as they have a significant role in shaping the bio-physical processes of the existing marine ecosystems (Clark et al., 2019; Cummings et al., 2018; Dayton et al., 2019; Gutt et al., 2019; Wan Hussin et al., 2019).

To achieve this goal, baseline surveys and continuous monitoring of natural ecosystems are urgently needed, as proposed by the 'Southern Ocean Observing System' (SOOS, 2017) and by the 'Scientific Committee on Antarctic Research' (SCAR, 2021) and discussed in the 'ANtarctic Terrestrial and Near-shore Observing System' report (ANTOS, 2015). Similar monitoring actions are also urged by the most important networks of marine observing systems, such as, for example, the 'Joint European Research Infrastructure network for Coastal Observatory' (JERICO), the 'European Multidisciplinary Seafloor and water column Observatory' (EMSO) and 'Ocean Network Canada' (ONC; Dañobeitia et al., 2020; Moran et al., 2019; Painting et al., 2020).

As suggested in Convey and Peck (2019), the most urgent actions to carry out are as follows:

- long-term and multidisciplinary evaluations of environmental change and the corresponding responses of the biota in terms of their distributions, physiologies, population ecosystem genetic structure modification and function;
- assessing how successful conservation measures are currently in the Antarctic marine environment, including programmes to collect the required data;
- expand the spatial and temporal resolution of oceanographic and biological measurements across the Southern Ocean.

For these reasons, there are many studies on the Antarctic marine environment aimed at collecting and analysing datasets extended in time, especially describing benthic fauna (Dayton et al., 2019; Pineda-Metz et al., 2020), fisheries (Watters et al., 2020) and plankton (Bolinesi et al., 2020; Cecchetto et al., 2021). Unlike the traditional survey programmes, operated through the direct intervention by the researchers in situ (e.g. research vessels, in situ measurements), automated and autonomous monitoring activities can collect large amounts of data, for periods extended in time, and in remote regions characterized by harsh conditions (Aguzzi et al., 2019; Rountree et al., 2020). Unfortunately, long-term and autonomous monitoring actions in Antarctica are still insufficiently practiced, and deal mainly with ice-sheet dynamics, iceberg tracking and meteorological data (Barbat et al., 2021; Ramesh & Soni, 2018; Rignot et al., 2019).

Among the methods for underwater environmental monitoring, video-based observation is increasingly being considered one of the most promising tools for environmental monitoring (Bicknell et al., 2016; Zampoukas et al., 2014). Nevertheless, underwater video monitoring in the Antarctic regions is not yet fully exploited, mainly due to the challenging in situ conditions and the high logistics costs of the survey campaigns and of the underwater instrument deployment. Examples of short-term video monitoring activities are the photogrammetry approach proposed in (Piazza et al., 2018, 2019, 2020) and the time-lapse cameras deployed for a few days in coastal areas, for observing benthic organisms (Kim et al., 2007; Peirano et al., 2016).

Within this context, this work presents and discusses a pilot study for an autonomous and long-term image-based monitoring activity, performed continuously from January to November 2017 in proximity with the Mario Zucchelli Station (MZS; Tethys Bay, 74°41.410′S, 164°06.233′E), Figure 1a,b. The monitoring activity was performed through a stand-alone imaging device (Figure 1c–e), specifically conceived for autonomous deployment extended in time (Corgnati et al., 2016; Marini et al., 2013; Marini, Corgnati, et al., 2018).

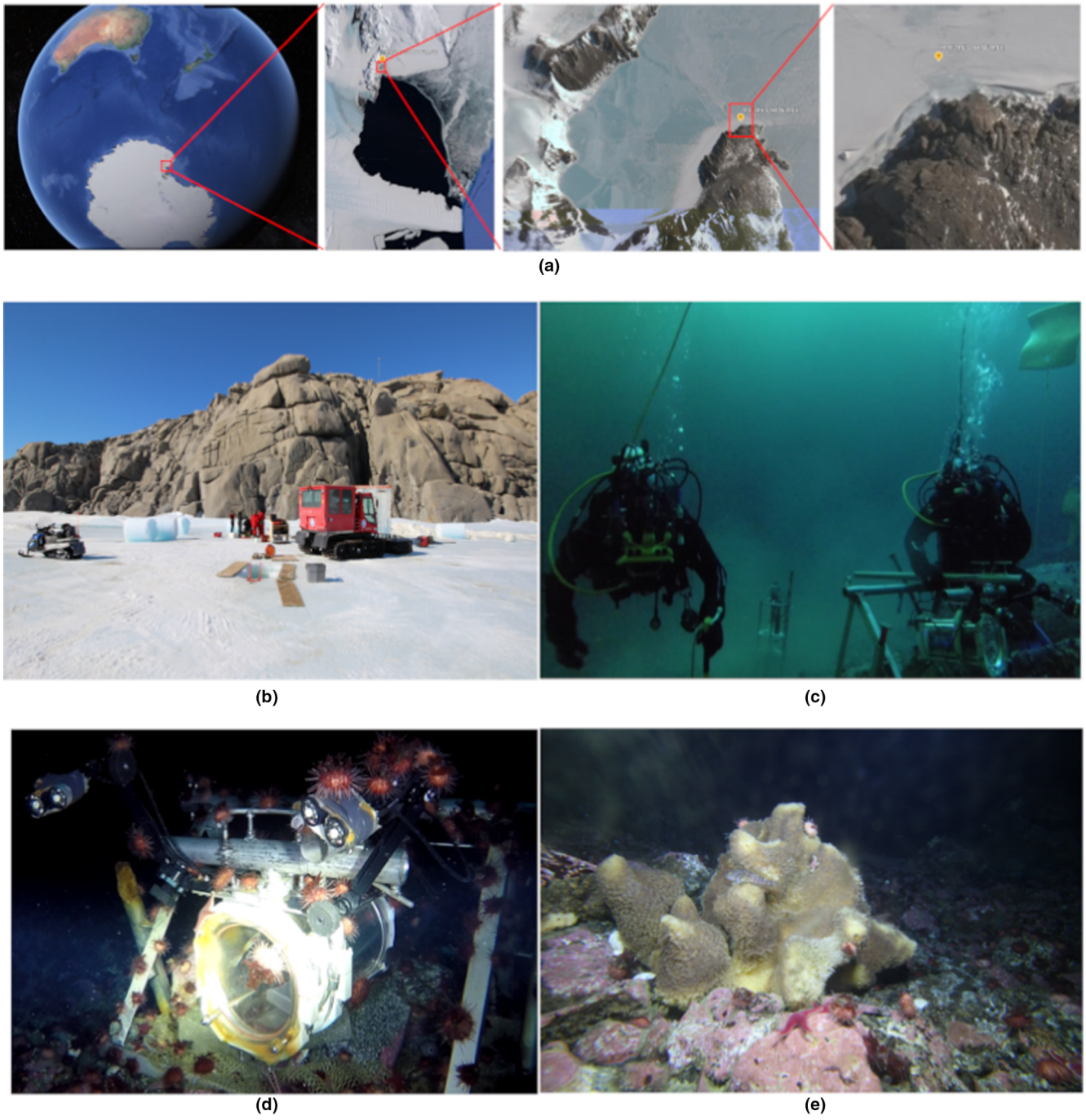


FIGURE 1 Overview of the monitored site. (a) Mario Zucchelli Station, Terranova Bay (Ross Sea) 74°41.410′S 164°06.233′E; (b) Surface of the deployment site; (c) Deployment on the seafloor; (d) The imaging device; (e) Example of image acquired by the imaging device using its own lighting system.

The autonomous imaging device was installed on a fixed platform on the seabed, in front of a granite cliff, facing NW, at a depth of 20 m. The device was programmed to acquire time-lapse images at 9-hr intervals of the sponge *Mycale* (*Oxymycale*) *acerata* Kirkpatrick, 1907 and of all the organisms surrounding the sponge during the monitoring period. This specific diving site, known as 'Zecca', was selected because of the availability of previous data on species distribution collected in the framework of previous expeditions and the presence of several prospering sponges. The site is also suitable for long-term experiments as the seabed is protected from the devastating ploughing effects of the icebergs.

After the recovery of the instrument, the acquired images were visually inspected to recognize the local species and to determine their temporal distribution along the monitoring period. Subsequently, the image dataset was analysed through computer vision and machine learning techniques. Results prove the effectiveness of the long-term automated visual monitoring of underwater extreme environments, acquiring data capable of presenting high

relevance scientific information otherwise not accessible with the state-of-the-art monitoring approaches commonly implemented in Antarctica. The discussion section shows how autonomous and intelligent imaging devices, based on the presented pilot study, can be used for gathering relevant ecological information in harsh and remote environments for automated observations extended in time.

## 2 | AUTONOMOUS IMAGING DEVICE

The imaging device used for the long-term monitoring was specifically designed and developed based on the European patent EP 2863257 B1 (Marini et al., 2013). The technology described in the patent consists of an intelligent imaging device capable to execute on board image processing algorithms and perform data communication. It is conceived for autonomous and stand-alone image-based monitoring in remote marine environments for deployments over extended periods of time, as discussed in Corgnati et al. (2016) and Marini, Corgnati, et al. (2018).

The imaging device used for the long-term monitoring performed in Antarctica was specifically implemented without communication and image processing facilities. This choice was motivated by the difficulty to transfer the acquired data outside the surface ice pack and also because all the acquired images were considered relevant. In fact, all the phenomena we could observe on the seabed was unknown and, as a consequence, the image processing flow was also unknown. The computational resources of the device were then used for performing a periodic backup of the acquired images, to a secondary internal memory storage component.

The imaging device implemented for the proposed pilot study was designed to be as simple as possible to ensure its functioning along the whole monitoring period in the extreme conditions of the Antarctic sea. Figure 2a shows the imaging device and its main components.

The acquisition component was a commercial Canon EOS 600D reflex camera equipped with a specifically designed firmware based on the Magic Lantern toolkit (Magic Lantern, 2021). The firmware allowed the automatic shooting of an image. The overall behaviour of the imaging device was defined by three different programmes, $P_0$, $P_1$ and $P_2$, coded at hardware level in the control component and selected through a magnetic switch activated by a diver operator during the deployment operations. A schematic explanation of the three programmes is shown in Figure 3. The device was equipped with a service display, visible through the transparent underwater case shown in 2c. During the execution of the programme $P_0$, a live view stream was redirected to the service display, to ease the diving operations of the deployment as shown in Figure 2d. The programmes $P_1$ and $P_2$ were characterized by two different standby time $T_1$ and $T_2$, for two different acquisition frequencies. The lighting system consisted of four high-performance LEDs embedded in epoxy resin and wired to the device underwater case, as shown in Figures 2a,d. The Control component was set to back up the camera every 100 acquired images, independently by the programmes $P_1$, and $P_2$. The processing component used in the pilot study was based on a Raspberry PI board (Raspberry Pi Foundation, 2021) and it was used for the periodic backup of the images acquired by the camera. The processing component was connected to the USB port of the Canon EOS 600D camera and during the backup, an automated script set up the connection to the camera for transferring only the images not yet backed up. Finally, an underwater wet connector allowed a diver operator to connect an external processing component (Figure 2b) to the processing component of the imaging device for downloading the acquired images without recovering the device. This functionality was particularly useful for checking the correct positioning of the device few days after the deployment.

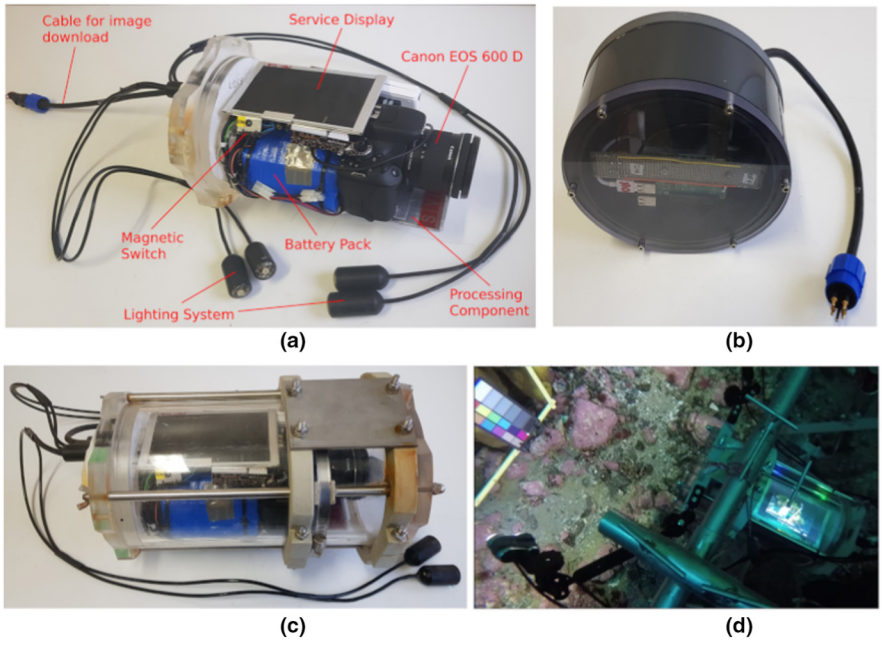


FIGURE 2 (a) The autonomous and stand-alone imaging device used for the pilot study; (b) The underwater external processing component used by the diver operator for downloading the acquired images without recovering the imaging device; (c) The imaging device inside its transparent underwater case; (d) The imaging device during the positioning in situ with the service display turned on.

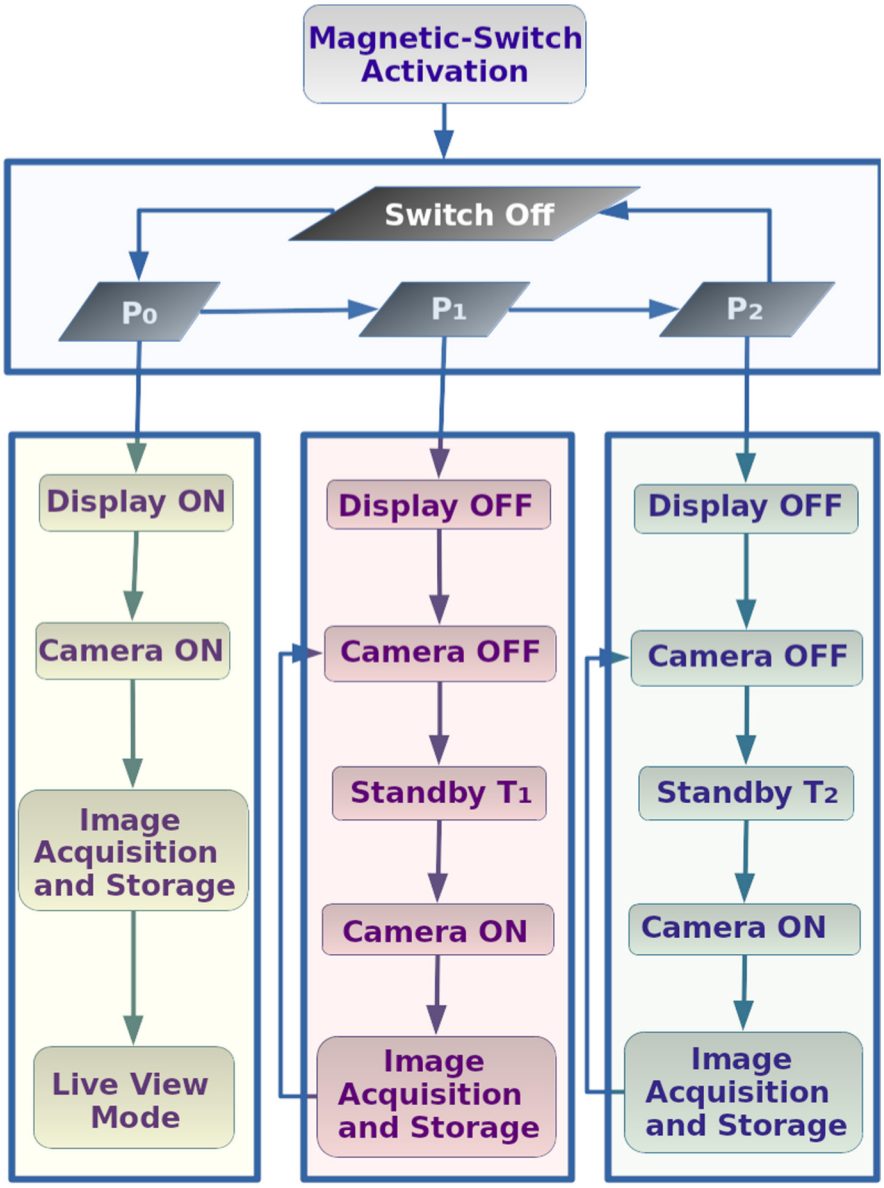


FIGURE 3 The three programmes for the positioning of the imaging device $P_0$, test $P_1$ and the operative monitoring activity $P_2$.

The most recent implementations of this device are conceived for a wider range of stand-alone monitoring applications and, although they are still based on the European Patent described in (Marini et al., 2013), they use more efficient and flexible hardware components. The described device is no longer based on a commercial camera: the acquisition component is now directly built on a PYXALIS CMOS sensor model HDPYX230-G, while the Control and the CPU components are specifically designed based on an ultra-low-power platform of the family NXP i.MX8 MINI, as detailed in OEngineering (2021).

## 3 | VISUAL INSPECTION OF THE IMAGES

During the monitoring period, from January to November 2017, the autonomous imaging device was installed on a fixed platform, at a depth of 20 m, as shown in Figure 1c,d. The device acquired one image every 9 hr, throughout the Antarctic summer, winter and the intermediate transition periods, for a total of 755 high-resolution colour images. Each image has a resolution of 5,207 × 3,469 pixels and was saved in the Canon proprietary raw format CR2 (CR2, 2021).

All the still images were acquired with a fixed field of view that allowed shooting the sponge *M. acerata* and the rocky area surrounding it, including the ice pack on the sea surface. An example of an acquired image is shown in Figure 1e.

After the recovery of the imaging device, the collected images were visually inspected and the framed organisms were counted, tagged and labelled. All relevant operational taxonomic units (OTUs) were first recognized by two trained biologists who compiled two independent classifications and, after having found the agreement on the identified OTUs, produced a visual list to instruct a manual annotator. Although there exist different software and web tools to support saving, managing, exploring, sharing and annotating marine imagery (Langenkämper et al., 2017; Rajesh & Lalitha Bhaskari, 2020;

Schoening et al., 2016; Zurowietz et al., 2018) for each image, all animals on the scene were manually annotated using the general purpose 'labelImg' software tool (LabelImg, 2021). For each specimen and for each image, the animal's bounding box and its OTU class were recorded. In cases of doubt, the animal's genus or family name was recorded instead of its species. Once all images were annotated, the same operator double-checked each image with the goal of upsampling possibly missed individuals.

Such a visual inspection resulted in the identification of 12 genera and 1 unclassified organism, as shown in Figure 4, where examples of specimens of each genera are presented.

During the visual inspection, a total of 23,881 organisms were counted, as summarized in Table 1. Note that the counts do not necessarily correspond to the exact number of individual animals. In general, it is not possible to establish whether two specimens present in two consecutive images are the same individual or two different individuals. On the contrary, as for example in the case of the unclassified organism shown in Figure 4e, it is probable that all the recorded counts correspond to the same individual staying almost in the same position for about 2 weeks. Nevertheless, the trend of the total animal counts and the temporal distribution of the species provide an useful insight into the observed fauna dynamics.

The duration of daylight is among the most important parameters driving the underwater faunal dynamics in the shallow coastal areas of Antarctica (Caputi et al., 2020; van Leeuwe et al., 2020). The average duration of daytime at the Mario Zucchelli Station was computed and discussed in Balog et al. (2019), yielding that from 3rd November to 7th February the sun is above the horizon for 24 hr continuously, while from 3rd May to 10th August natural light is completely absent.

The changes in natural light affect the field of view of the acquired images, possibly affecting the visual counting in the furthest regions not sufficiently reached by the device lighting system. To avoid any potential bias due to the reduction of the field of view, the fauna dynamics presented were analysed by considering only the image regions constantly illuminated by the imaging device. This was obtained by masking the image regions not involved in the analysis and considering only the tags intersecting the unmasked region of the image. Figure 5a shows the total counts of the specimens for each image, together with the corresponding long- and mid-term trends, and an example of a masked image (Figure 5b–d).

A diagram of the total counts of the animals, restricted to the masked images, is shown in Figure 5a (black line). It shows that a large number of individuals are present until the end of February. This massive presence is due to the huge phytoplankton bloom produced when the sea surface is not covered by the ice pack (van Leeuwe et al., 2020). The quite evident drop in the counts following this phase (beginning of March) is not related to a sudden lack of organisms, but rather to the temporary presence of biofouling on the camera, following the phytoplankton bloom. The long-term trend (red dashed line) is computed through the LOWESS (LOcally WEighted Scatterplot Smoothing) approach, resulting in a concave curve with its minimum value near the end of the Antarctic night, represented by the two green vertical lines. This trend shows an

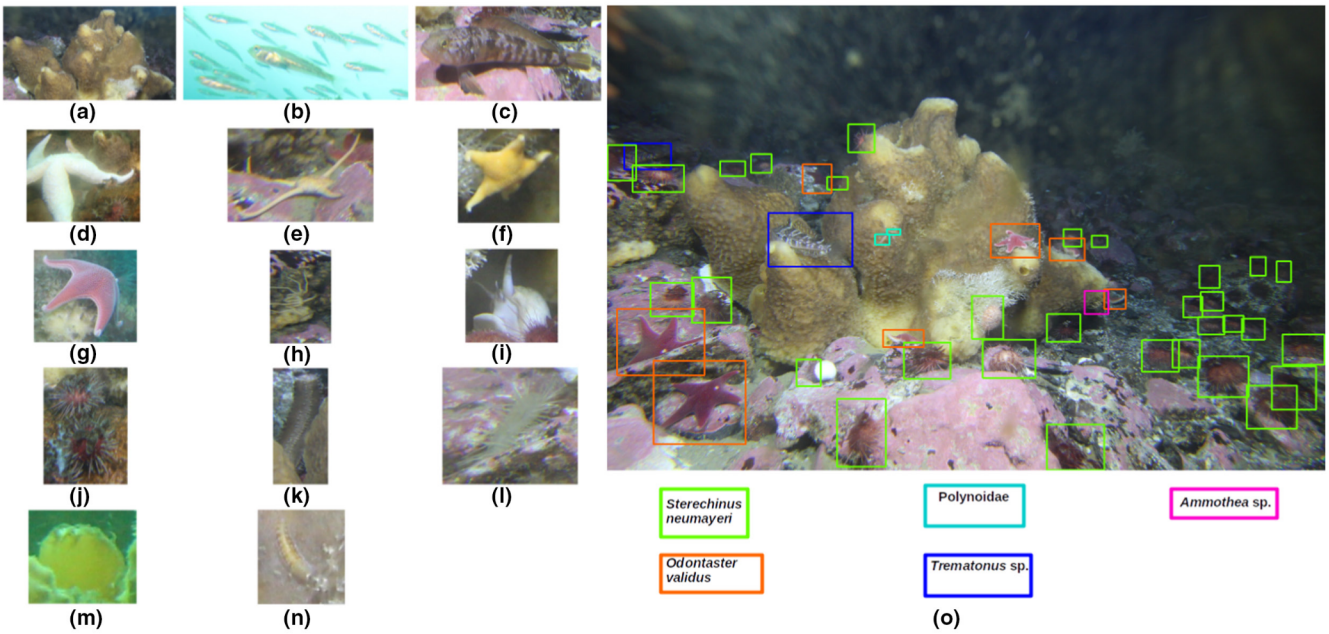


FIGURE 4 Examples of species detected during the monitored period. (a) *Mycale (Oxymycale) acerata* Kirkpatrick, 1907; (b) *Trematomus newnesi* Boulenger, 1902; (c) *Trematomus* sp.; (d) *Diplasterias brucei* (Koehler, 1907); (e) Ophiuridae; (f) *Odontaster* sp.; (g) *Odontaster validus* Koehler, 1906; (h) *Ammothea* sp.; (i) *Neobuccinum eatoni* (E. A. Smith, 1875); (j) *Sterechinus neumayeri* (Meissner, 1900); (k) *Staurocucumis turqueti* (Vaney, 1906); (l) *Flabegraviera mundata* (Gravier, 1906); (m) Unclassified; (n) Polynoidae. (o) An example of a manually tagged image, containing 31 specimens of *S. mneumayeri* (green rectangle), 7 specimens of *O. validus* (orange rectangle), 2 specimens of Polynoidae (cyan rectangle), 2 specimens of *Trematomus* sp. (blue rectangle), 1 specimens of *Ammothea* sp. (pink rectangle).

increase in organism counts at the two extreme bounds of the time series, corresponding to the most illuminated period of the year. The mid-term LOWESS trend (blue line) shows an oscillating signal with a non-constant frequency, suggesting that the observed abundance dynamics might depend on environmental parameters different from the natural light.

**TABLE 1** Distribution of image tags per species

| Species | Number of Tags |
|---|---|
| *Sterechinus neumayeri* (Meissner, 1900) | 16,605 |
| *Odontaster validus* Koehler, 1906 | 5,965 |
| *Trematomus newnesi* Boulenger, 1902 | 401 |
| *Trematomus* spp. | 267 |
| Polynoidae | 143 |
| *Odontaster* spp. | 139 |
| *Diplasterias brucei* (Koehler, 1907) | 137 |
| Ophiuridae | 79 |
| *Ammothea* sp. | 70 |
| *Neobuccinum eatoni* (E. A. Smith, 1875) | 23 |
| Unclassified | 21 |
| *Staurocucumis turqueti* (Vaney, 1906) | 17 |
| *Flabegraviera mundata* (Gravier, 1906) | 14 |
| Total tags | 23,881 |

The most observed species in the acquired images are the sea urchin *Sterechinus neumayeri* (Meissner, 1900) and the sea star *Odontaster validus* Koehler, 1906. These organisms are recorded as being abundant in all the acquired images and they are both present on the sponge and on the rocky bottom. The other observed species have a different temporal distributions, as shown in Figure 6, where the animal counts per species refer to the masked images and are grouped into bi-weekly temporal slots.

The species distribution shows that the *S. neumayeri* and the *O. validus* are the ones responsible for the concave shape of the long-term trend in the total count diagram. *Trematomus* spp. are present over the whole period, although a noticeable increase is recorded from the beginning of the Antarctic night until the end of the time series. A similar behaviour can be observed for the Polynoidae, the sea stars *Odontaster* spp. and the sea spider *Ammothea* sp., that occur occasionally until May for increasing their presence since the beginning of the dark period and in the following one. In contrast, the sea cucumber *Staurocucumis turqueti* Vaney, 1906 appears only in the daylight periods, in the second week of observation and just after the Antarctic night. The fish *Trematomus newnesi* Boulenger, 1902 is abundant in the surroundings of the sponge only in the first 2 weeks of observation, as well as the unknown species observed in the same weeks. The sea cucumber *Flabegraviera mundata* (Gravier, 1906) appears rarely, both in the daylight period and in the dark period. Similarly, the gastropod *Neobuccinum eatoni* (E. A. Smith, 1875) and the sea star *Diplasterias*

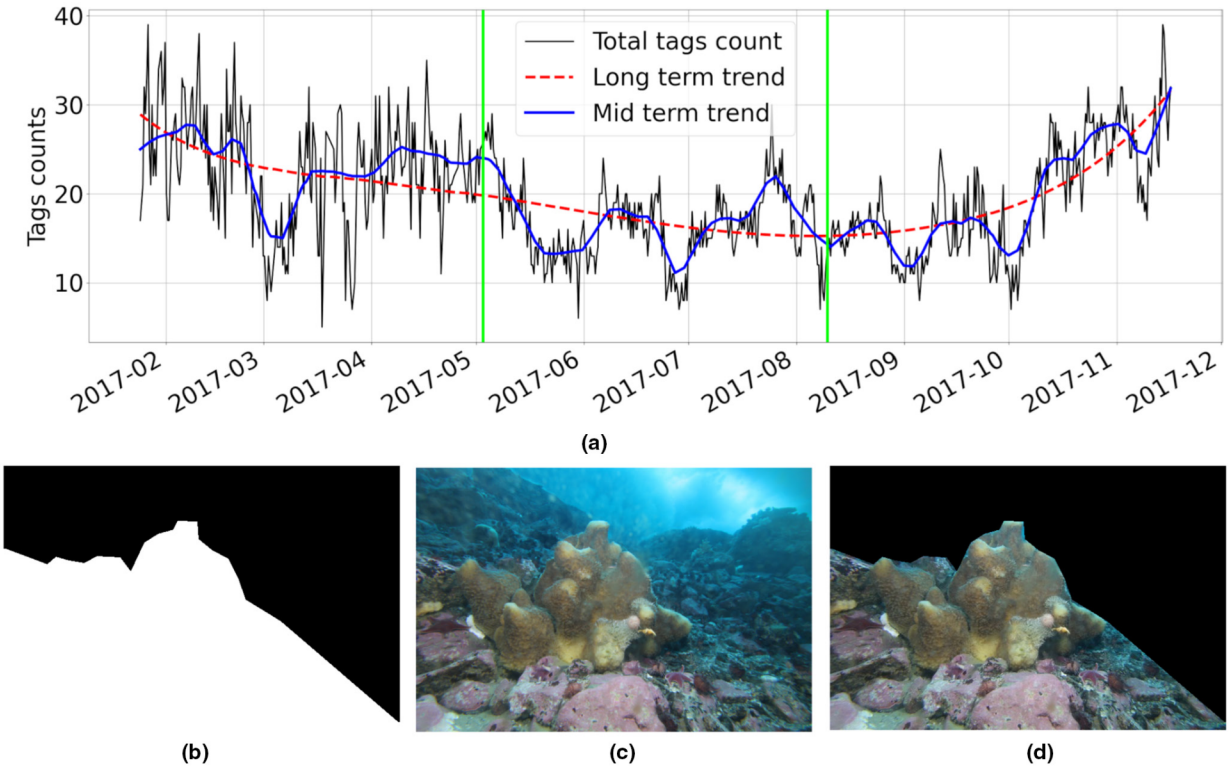


**FIGURE 5** (a) The total count of the organisms (black line), the corresponding long-term LOWESS trend (dashed red line) and the mid-term LOWESS trend (blue line), the two vertical lines refer to the beginning and end of the Antarctic night, respectively; (b) The mask binary image; (c) an example of acquired image; and (d) the corresponding masked example.

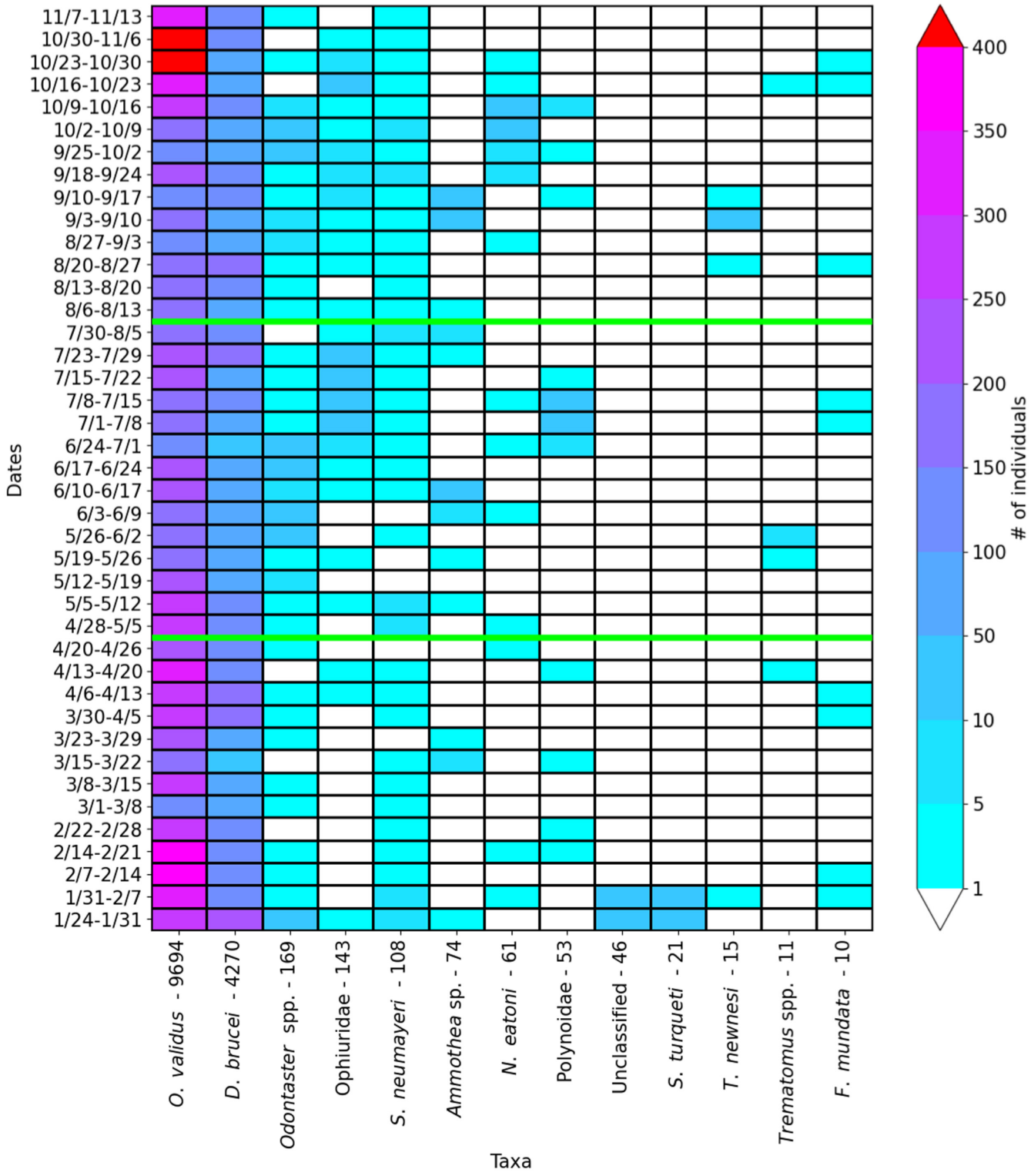


FIGURE 6 Bi-weekly distribution of the image tags, with respect to the species present in the acquired images. The two horizontal green lines correspond to the beginning and end of the Antarctic night period according to Balog et al. (2019). Along the species/genus are reported the number of tagged individuals.

*brucei* (Koehler, 1907) are abundant all over the year, in particular an adult of the sea star, whose size is noticeably larger than the average size of the other specimens (more than 20 cm in diameter), is observed in February.

## 4 | AUTOMATED IMAGE ANALYSIS

The acquired images have a significant information content, but a visual inspection for extracting such information would need a

considerable effort in terms of human resources. In contrast, algorithms for automated content-based image analysis can be used for extracting accurate and measurable knowledge from the acquired data, with little human effort required (MacLeod et al., 2010; Malde et al., 2019; Marini, Fanelli, et al., 2018).

Such automated approaches are gaining a growing consensus within the marine sciences community, becoming an established scientific tool for transforming underwater cameras into effective ecologic sensors (Aguzzi et al., 2020; European Marine Board, 2020; Jahanbakht et al., 2021; MacLeod et al., 2010; Malde et al., 2019; Marini et al., 2018). For this reason, besides visual inspection, computer vision and machine learning algorithms have been used for analysing the acquired images.

After the recovery of the autonomous imaging device, the collected images were analysed with the aim of estimating (a) the underwater environmental light changes; (b) the organisms activity dynamics; (c) the sponge activity; and (d) the automated detection of sea stars and sea urchins. Since the proposed processing algorithms are independent by the specific Antarctic application and by the used imaging device, they can be used for analysing different image datasets. To facilitate the reuse of the implemented analysis algorithms, the supporting information provide the user manual for executing the proposed algorithms.

## 4.1 | Underwater diffused light

The diffused light reaching the seabed through the ice pack does not correspond directly to the daylight dynamics discussed in Balog et al. (2019). For example, the accumulation of snow on the sea pack or the shadow projected by cliffs surrounding the studied area can locally change the underwater light dynamics. The underwater diffused light is estimated by combining the Dark Channel Prior (DCP) and Bright Channel prior (BCP) approaches (Dark Channel Prior Dehazing, 2015;Peng et al., 2018; Shi et al., 2018). DCP and BCP are based on the general assumption that the diffusion of the light depends on the particulates suspended in a medium (e.g. the water column), whose back-scattering distorts the colours and reduces the contrast between the objects in the scene (Peng et al., 2018; Shi et al., 2018).

Assuming that the light attenuation is homogeneous, the intensity $I^c(x)$ in the image colour channel $c$ at the pixel $x$ is defined by Equation (1; Peng et al., 2018):

$$I^c(x) = J^c(x)t(x) + A^c(1 - t(x)), \quad c \in \{r, g, b\}, \tag{1}$$

where $J^c$ is the scene radiance, $A^c$ is the ambient light, $t$ is the transmission function and $c$ is one of the RGB image channels. The scene radiance is the light reflected by the objects in the scene, the transmission function describes the portion of the scene radiance which is not scattered or absorbed by the medium and which reaches the camera.

The DCP assumes that the image pixels corresponding to a smaller transmission value are affected by a hazing that attenuates the differences between the intensities of the pixels in all three image channels (Peng et al., 2018). According to this assumption, for each pixel $x$ in the acquired image, the DCP approach defines the dark channel radiance as the minimum value among RGB channels in a local patch $\Omega(x)$ centred at $x$, as defined in Equation (2) (Peng et al., 2018):

$$J^{\mathrm{RGB}}_{\mathrm{DCP}}(x) = \min_{y \in \Omega(x)} \left\{ \min_{c \in \{r,g,b\}} J^c(y) \right\}. \tag{2}$$

The less the light reaching the pixel $x$ is affected by the back-scattering, the more its dark channel radiance $J^{\mathrm{RGB}}_{\mathrm{DCP}}(x)$ tends to zero. The dark channel image $I^{dcp}(x)$ is defined by substituting $J^c(x)$ with $J^{\mathrm{RGB}}_{\mathrm{DCP}}(x)$ in Equation (1). As a consequence, the term $J^{\mathrm{RGB}}_{\mathrm{DCP}}(x)t(x)$ tends to zero for the pixels not affected by back-scattering, while brighter pixels correspond to the diffused ambient light $A$, as their values only come from the term $A^c(1 - t(x))$. The amount of diffused light in the image is computed by selecting a subset of brightest pixels in the dark channel image $I^{\mathrm{DCP}}(x)$ and computing their average intensity (Peng et al., 2018; Shi et al., 2018).

In the case of the images acquired during the Antarctic night, the diffused ambient light is absent but the computed dark channel image $I^{\mathrm{DCP}}(x)$ is not completely dark. The dark channel corresponding to such images has brighter pixels corresponding to the light diffused by objects in the scene (i.e. the sponge, the rocky bottom, the biofouling on the camera) illuminated by the lighting system of the imaging device. The misleading effect of these pixels is mitigated by computing the BCP image and combining it with the DCP image. Based on the same assumption used for the computation of the DCP of the image, the BCP radiance is defined by Equation (3) (Shi et al., 2018):

$$J^{\mathrm{RGP}}_{\mathrm{BCP}}(x) = \max_{y \in \Omega(x)} \left\{ \max_{c \in \{r,g,b\}} J^c(y) \right\}. \tag{3}$$

Unlike the radiance defined in Equation (2), the less the light reaching the pixel $x$ is affected by back-scattering, the more the bright channel radiance $J^{\mathrm{RGP}}_{\mathrm{BCP}}(x)$ tends to its maximum value (i.e. 1 in the case of the present implementation). This means that the BCP image $I^{\mathrm{BCP}}(x)$, obtained by substituting the radiance $J^c(x)$ with $J^{\mathrm{RGP}}_{\mathrm{BCP}}(x)$ in Equation (1), has brighter pixels corresponding to regions where either the light is not affected by back-scattering or regions where the diffused light has higher values. The Corrected Dark Channel Prior (CDCP) image is then defined by Equation (4):

$$I^{\mathrm{CDCP}}(x) = \max\left\{0,\ I^{\mathrm{DCP}}(x) - \alpha I^{\mathrm{diff}}(x)\right\}, \quad I^{\mathrm{diff}} = \left| I^{\mathrm{DCP}}(x) - I^{\mathrm{BCP}}(x) \right|, \tag{4}$$

where $\alpha$ is a real number varying in the range $[0, 1]$ and the image difference $I^{\mathrm{diff}}(x)$ between the dark and bright channel images has brighter pixels corresponding only to regions where the light is not affected by back-scattering (i.e. low values of diffused light) and dark pixels corresponding to regions characterized by diffused ambient light. The brighter pixels (if any) in the CDCP image represent

regions characterized by the ambient diffused light (if any), as shown in Figure 7, independent of whether the scene was illuminated by the lighting system of the imaging device or by the natural ambient light.

The underwater diffused light is obtained by resizing the acquired images to 640 × 427 pixels. The size of the local patch $\Omega(x)$ is 101 pixels (image padding is used for analysing the image borders), the value of the $\alpha$ parameter in Equation (4) is set to 0.5 and the estimated light intensity is computed by considering only the brightest 30% of the pixels of the CDCP image.

Figure 7 shows two examples of diffused underwater ambient light estimates, based on the CDCP image defined in Equation (4), where the computed values correspond to 0.91 and 0.24, for the daylight image a) and the night image d) respectively.

Figure 8a shows the relative value of the estimated diffused light, computed for each image over the monitored period. The maximum value corresponding to 1 refers to the brightest images in the dataset, while darker images have a smaller estimated diffused light value. The two vertical lines correspond to the beginning and end of the Antarctic night as presented in Balog et al. (2019). The blue line is the trend of the estimated diffused light, computed as the moving average of the obtained light values.

Although the sun is constantly present above the horizon from the beginning of November to the beginning of February, the monitored site shows a daily light/shadow cycle for the largest part of the Austral daylight period. As discussed in Peirano et al. (2016), the shadow effect is caused by the position of the cliff with respect to the monitoring site and such a light variation has been captured by image analysis algorithms.

The diagram in Figure 8a shows the light/shadow cycle, as an alternation between higher and lower values, together with a decreasing trend of the diffused light until the beginning of the Antarctic night (first green vertical line), even with some discontinuities caused by biofouling on the camera. The small noisy light variations shown in the dark period are mainly originated by some residual biofouling present on the camera as shown in Figure 7f. After the end of the Antarctic night (second green vertical line), the natural light increases, with some discontinuities, until the end of September, when a significant decrease happens, yet probably caused by a cloudy sky or by the accumulation of snow on the ice pack.

## 4.2 | Seabed organisms' activity

This analysis is aimed at the automated detection and counting of the organisms' movement during the observation period. From two consecutive images, it is possible to detect how many organisms moved from their position, or entered or exited from the observed scene. As the imaging device was installed on a fixed platform, the image background is also fixed; thus, the movement of the foreground organisms is detected by applying an image differencing technique (Marini et al., 2018; Moeslund, 2012).

The proposed image differencing algorithm is an unsupervised image processing technique not requiring any special training effort, as in the case of the supervised machine learning approaches. As a consequence, no visual inspection is needed either. It is based on an appropriate image segmentation process capable of identifying

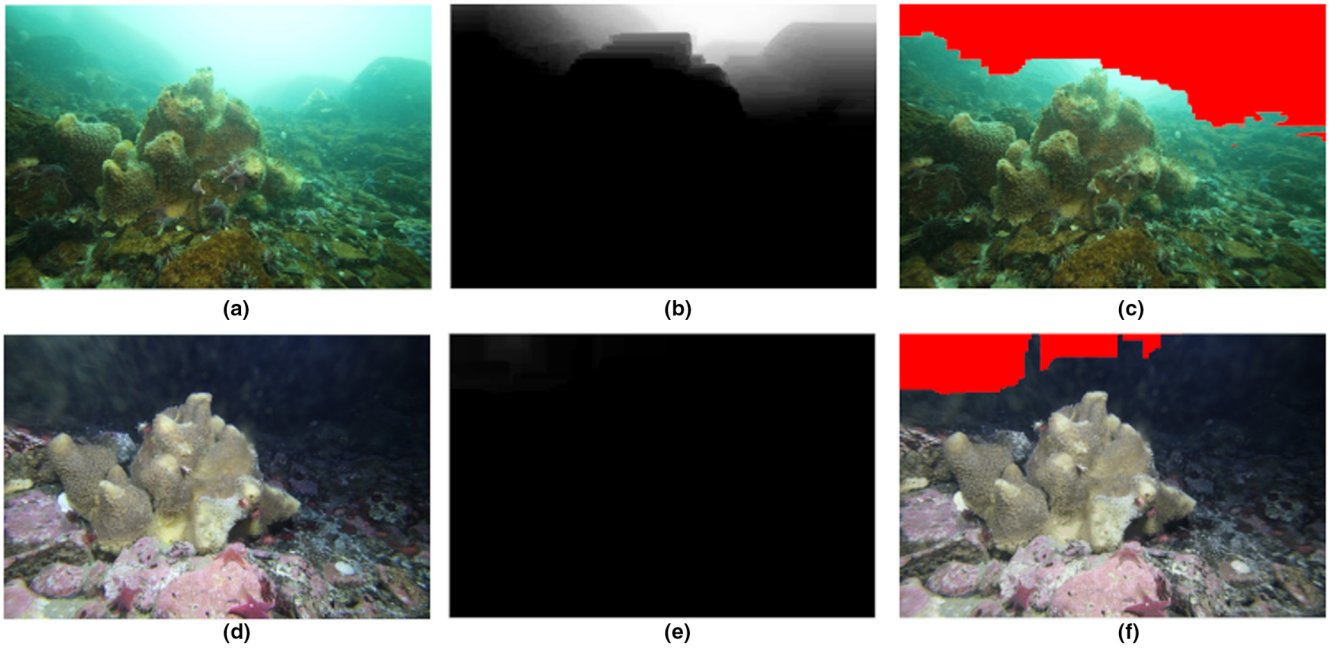


FIGURE 7 Image examples showing the estimate of the underwater, diffused ambient light analysis. The images in (a and d) were acquired during the Antarctic daylight and the night period, respectively; (b and e) represent the Corrected Dark Channel Prior (CDCP) images, respectively; (c and f) show the image regions (red areas) contributing to the estimate of the diffused light.

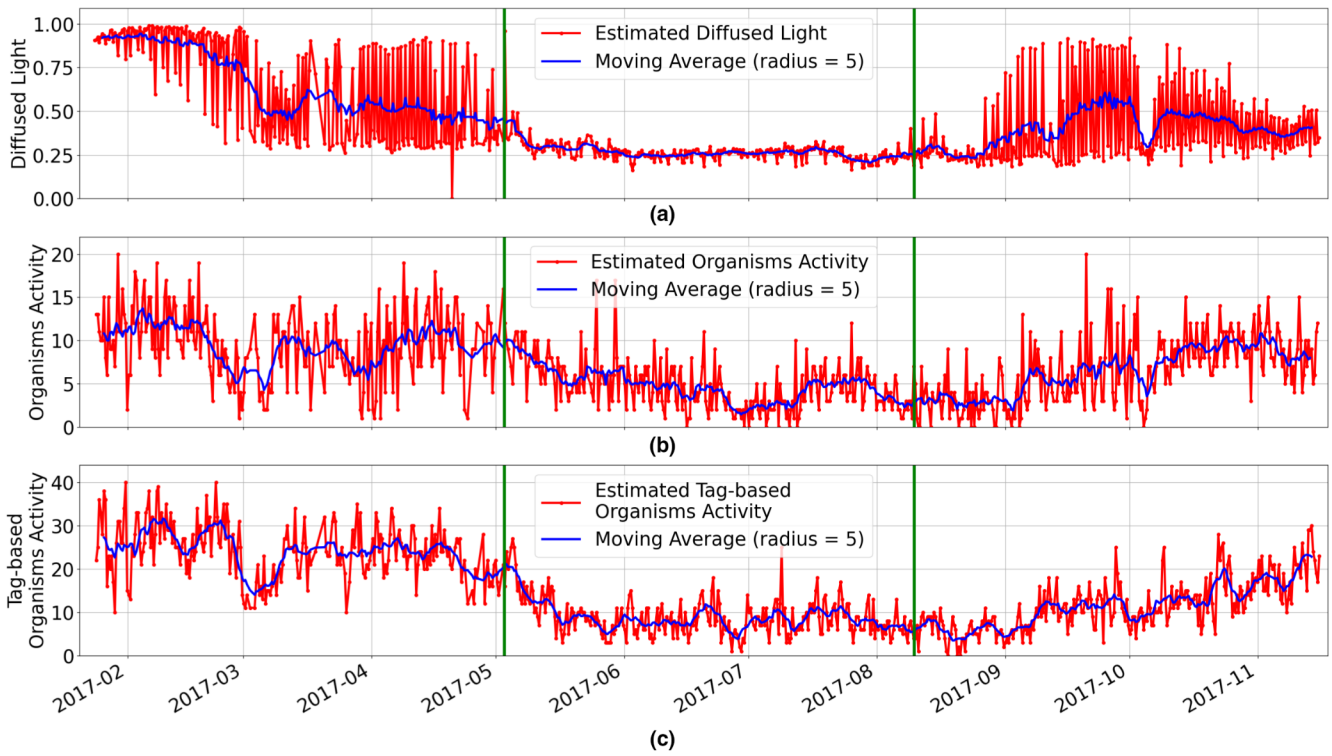


FIGURE 8 (a) Reconstruction of the underwater diffused light. The ordinate axis represents the relative light intensity, where 1 is the maximum light value estimated in the whole image dataset and 0 is the complete absence of diffused light. (b) Computation of the organisms' activity based on the image differencing approach. The ordinate axis represent the number of computed movements between two consecutive images. (c) Computation of the organisms' activity based on the image tags obtained through visual inspection. The blue lines in the three diagrams represent the moving average with radius equal to 5.

the relevant subjects (i.e. the organisms moving on the seabed) and detecting their movements.

The segmentation process is based on two assumptions: (i) the relevant subjects within an image (i.e. the organisms moving on the seabed) move faster than the irrelevant image regions consisting of the static background (e.g. the sponge, the rocky bottom); (ii) the images are sorted with respect to the acquisition time (i.e. the image dataset is organized as a time series).

Based on the two previously defined assumptions, the image differencing approach involves three consecutive images, as defined in Equation (5):

$$I^{\text{diff}} = |I_t - I_{t-1}| \wedge |I_t - I_{t+1}|, \tag{5}$$

where the operator – represents the difference between two images, the operator ∧ represents the pixelwise logical AND operation between two images, and the indices $I_{t-1}$, $t$ and $I_{t+1}$ represent the time-stamps of three consecutive acquired images (Moeslund, 2012).

After the image difference is computed, a blurring operator, a Gaussian threshold and morphological operators (Marini et al., 2018; Moeslund, 2012) are applied to identify the image blobs representing potentially relevant subjects.

Figure 8b shows the computed activity of the benthic fauna, obtained through the image differencing approach. Since the field of view of an image depends on the ambient light, which may vary, the automated image analysis is again restricted to the region of the images constantly illuminated by the device lighting system, as shown in Figure 5b. This region includes the sponge and the rocky bottom in front of it. The ordinate axis of the diagram shows the number of movements of the organisms and the red line represents the movements computed in each image with respect to the previously acquired image. The blue line represents the trend of the organisms' activity, computed as a moving average.

Figure 8b shows that the faunal activity noticeably decreases during the Antarctic night, increasing again with the increasing of the duration of daylight, suggesting that this faunal activity is mainly driven by the seasonal variations in the light.

To assess the performance of the automated movement counts, the differencing approach applied to the acquired images is also applied to the image tags obtained through a visual inspection restricted to image regions illuminated by the imaging device. The results of the tag-based estimation of the movements of the organisms are shown in Figure 8c. The resulting diagram is strongly correlated to the one shown in Figure 8b, sustaining the hypothesis that the detection of faunal activity can be performed automatically with an accuracy comparable to that obtained through a huge visual effort. Indeed, the Pearson correlation coefficient between the two moving averages (blue lines) is equal to 0.86 ($p$-value = $7.4e^{-222}$).

### 4.3 | Oscula activity

Another automated image analysis is performed to investigate the activity of the sponge *M. acerata* over the entire period of observation. In particular, the activity of four sponge oscula is analysed to estimate their dilatation and contraction activity by computing the circle fitting the border of each osculum.

The oscula of the sponge are quite small in size with respect to the whole image and when contracted they reduce their radius until they disappear, becoming almost indistinguishable from the other parts of the sponge. Due to the high resolution of the imaging device camera (5,207×3,469 pixels), it is possible to zoom into the acquired images to capture the details needed to estimate their dilatation/contraction dynamics. The four oscula are analysed using image masks aimed at cropping to the smaller regions containing the oscula. Then the Hough circle transform function implemented in OpenCV (OpenCV, 2021) is used to identify the border of an osculum, in each cropped image, together with the diameter of the corresponding fitting circle.

The cropped images have a very small size and small changes of the position of the imaging device noticeably affect their content. For example, the mask used for the osculum 1 has size 74×82 pixels, while the mask used for the osculum 2 has size 66×58 pixels. Actually, after the acquisition of the first 109 images (out of 755 images), the imaging device moved slightly toward down and right, producing an offset of a few pixels (30×108 pixels) in the position of the sponge with respect to the borders of the image. To compensate for this small offset, two masks for each oscula are needed, one before and one after the movement of the device.

Since no osculum is a perfect circle, and since its geometry changes during the dilatation/contraction process (Figure 9b) the Hough circle transform is executed by searching all the fitting circles with minimum radius corresponding to 5 pixels and maximum radius corresponding to 50 pixels. The fitting circle of each cropped image is then computed by averaging both the computed circle centres and radii.

Figure 9a shows the sponge and the four analysed oscula. Figure 9b shows the sequence of (not contiguous) image crops of the osculum 3, with different dilatation and contraction levels. Figure 9c shows the same image sequence where the fitting circle of the osculum is automatically computed.

The activity of the oscula is shown in Figure 10. The red dots represent the osculum aperture expressed as the diameter of the fitting circle, the blue line represents the osculum dilatation/contraction trend computed as a moving average.

Although the four oscula have different dynamics, all of them share a similar behaviour with respect to the Antarctic day/night alternation. Before the beginning of the Antarctic night (left green vertical line), the four oscula are contracted for most of the time (i.e. the diameter is approximately equal to 0). In particular, the computed diameter is equal to 0 for 92%, 76%, 51%, 80% of the analysed images, for oscula 1–4, respectively. In contrast, during the Antarctic night period (between the two vertical green lines), all the oscula reach the maximum dilatation for the majority of the time series and the percentage of contracted oscula drops down to 13%, 32%, 13%, 48% for oscula 1–4, respectively. In the period following the Antarctic night, the number of images having a computed osculum radius equal to 0 increases to values similar to the period preceding

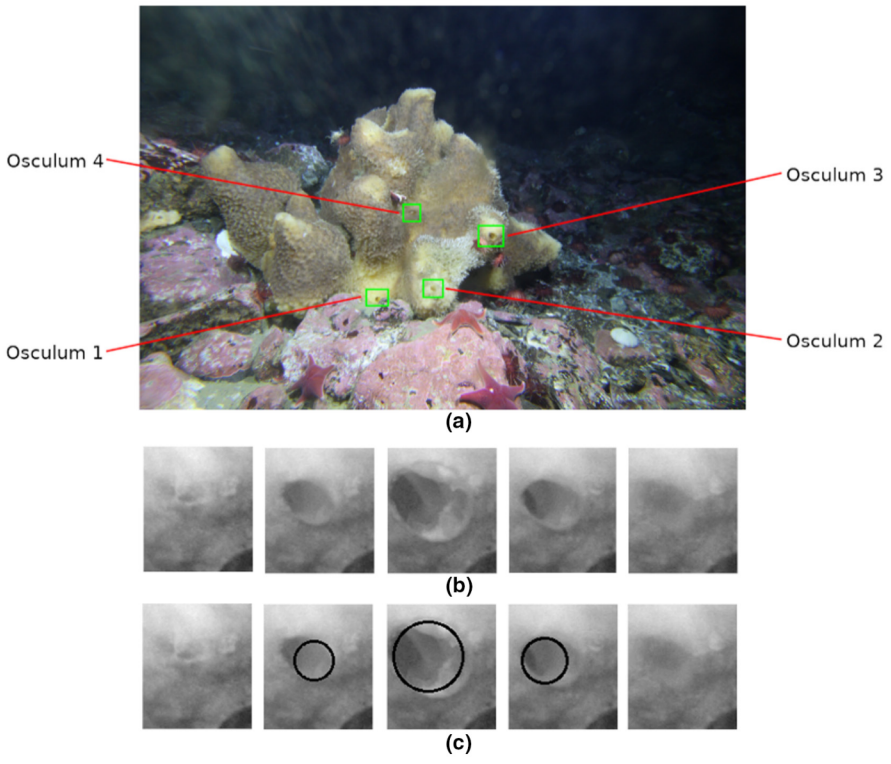


FIGURE 9 (a) The four oscula used for analysing the sponge dynamics; (b) Sequence of images representing the oscula dilatation and contraction; (c) Circles computed for estimating the aperture of the oscula.

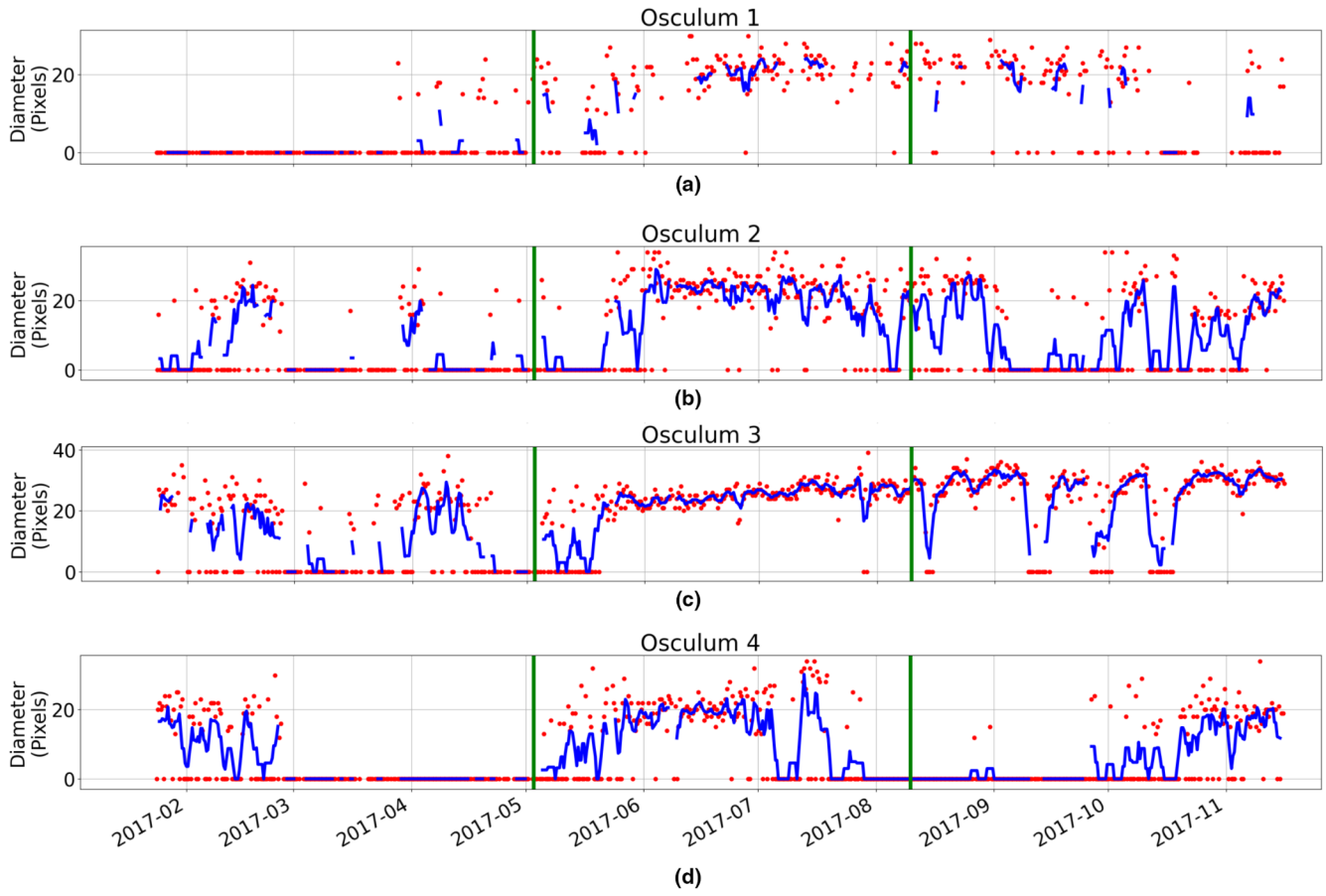


FIGURE 10 The dilatation/contraction activity estimated for: (a) osculum 1; (b) osculum 2; (c) osculum 3; and (d) osculum 4. The red points represent the diameter of the circle fitting the osculum, the blue line represents the moving average (with radius 5) of the computed diameters.

the Antarctic night, although with significant differences. In this period, the percentage of contracted oscula is equal to 36%, 54%, 14%, 74% for oscula 1–4, respectively. In particular, an oscillation is evident for oscula 2 and 3.

## 4.4 | Automated detection of organisms

Manual tagging through visual inspection is an expensive activity requiring significant human effort. Nevertheless, the knowledge obtained from such a visual activity can be used for training a supervised classifier based on machine learning for automatically recognizing and counting the organisms captured in the images (Langenkämper et al., 2020; Lopez-Vazquez et al., 2020; Malde et al., 2019; Marini, Fanelli, et al., 2018). The sea urchins and the sea stars are the most present species in the acquired images and a convolutional neural network based on the YOLO architecture (Redmon et al., 2016; Srivastava et al., 2021) is trained for demonstrating the effectiveness of the automated detection of specimens from these two species.

The image-content classifier used for the automated detection of the sea stars and the sea urchins is the YOLO-V5 convolutional neural network, freely available from the GitHub software repository (YOLO V5, 2021). Taking advantage of the transfer learning approach (Zhuang et al., 2021), the YOLO-V5 classifier is pre-trained for the object detection task on the general purpose COCO dataset (COCO, 2021). Then the classifier is specialized for the two studied species by re-training it three times using the last estimated weights as pre-trained input, for the next iteration, and successively increasing the image resolution from 128 to 480 pixels. The performance of the classifier is assessed through K-fold cross-validation summarized by the average of the Average Precision (AP) on the sea star class and the sea urchin class, as defined in Fawcett (2006).

All the image tags obtained from the visual inspection (i.e. not only the tags corresponding to the masked regions of the images) are randomly sampled and split into two sets, one used for training and validation and the other for testing. The training-and-validation set consists of 14,163 sea urchin specimens and 5,115 sea star specimens sampled from 642 images. A fivefold cross-validation (Dougherty, 2013; Kohavi, 1995) is used to evaluate the classification performance, finding a mean average precision of 82% (standard deviation 0.07) computed with an Intersection over Union (IoU) corresponding to 0.5 (Zhu et al., 2021). The best performing classifier

obtained through the cross-validation is then applied to the test set, consisting of 964 sea stars and 3,029 sea urchins. The test set mean average precision at 0.5 IoU is 92%.

Figure 11a shows several examples of YOLO classifications performed on the test set under different conditions of underwater diffused light. Figure 11b compares the YOLO automated detection, performed on the test set (solid blue line), with the sea stars and sea urchins tags obtained from the visual inspection (red dashed line). The Pearson correlations between the automated detections and the specimens' tags obtained from the visual inspection are 0.89 ($p$-value = $2.4e^{-39}$) and 0.85 ($p$-value = $6.9e^{-33}$) for the sea stars and the sea urchins, respectively.

## 5 | DISCUSSION AND CONCLUSIONS

One of the most urgent tasks for the coming decades is the development of technologies for continuously tracking and accurately predicting the biological responses to human impacts and global climate changes, especially in the continent of Antarctica (Brasier et al., 2019; Clark et al., 2019; Convey & Peck, 2019). Within this context, high-definition still and video image data constitute a key non-destructive approach for the non-invasive monitoring of aquatic marine environments (Aguzzi et al., 2019; Bicknell et al., 2016; Jahanbakht et al., 2021). Many studies in the literature contributed to the analysis of benthic fauna outside the Antarctic region (Lopez-Vazquez et al., 2020; Möller & Nattkemper, 2021), including the analysis of corals (Osterloff et al., 2019; Zuazo et al., 2020) and sponge dynamics (Harrison et al., 2021; Möller et al., 2019).

The imaging device used in this pilot study is a simplified version of a class of more complex devices that can operate autonomously for extended periods of time and are capable of extracting and transferring the relevant information contained in the acquired images (Corgnati et al., 2016; Marini et al., 2013; Marini, Corgnati, et al., 2018). The use of this kind of device in remote sites characterized by difficult deployment operations, like the Antarctica's benthic habitat, is crucial for gathering long-term data capable of explaining the functioning of the ecosystem.

The hardware architecture of a device capable of executing algorithms for content-based image interpretation, independently of remote computational resources, is the core of the edge-computing paradigm (Shi et al., 2016). Within this paradigm, unlike cloud computing, the data do not need to be transferred outside the device to be processed. On the contrary, the data are processed as close as possible (possibly onboard) to the source that generated them. Such onboard intelligence can be used for adaptively changing the behaviour of the imaging device in a way that depends on the occurrence of relevant triggering events. For example, changes in the diffused underwater light, as shown in Figure 8a, can be used as triggering events for increasing (decreasing) the frequency of the image acquisition. Similarly, the acquisition frequency can be adapted depending on the observed fauna's activity, as shown in Figure 8b. For example, when the device detects relevant changes in the fauna's movements, it can adapt its behaviour so as to minimize the risk of data downsampling (oversampling). The imaging device is also capable of executing image classification algorithms (see Figure 11) specifically designed to be executed on hardware components with limited computational capacity (Marini, Fanelli, et al., 2018). In this case, the behaviour of the device can change when a target organism enters (exits) the scene or when the number of its occurrences reaches a fixed threshold.

Underwater communication of information to a land station is rarely practiced in Antarctica, especially because of the difficulties of placing a surface antenna when the ice pack is unstable. However, when the sea surface is free of ice or when it is completely frozen, underwater observing systems can transfer the acquired data through appropriate surface communication facilities (Jahanbakht et al., 2021). In this case, the double link communication capability of the imaging device could be used either for the periodic transmission of relevant information from the device (e.g. image sub-regions, abundance time series) or for receiving new configuration programmes and image processing algorithms.

The imaging device deployed in this pilot study showed its potential for the investigation of the seasonal dynamics of macrobenthos. The species recognized in the image time series were already known for Tethys Bay (Vacchi et al., 2000). The fish *T. newnesi* was observed near the sea bed only at the beginning of the observation period (end of January, beginning of February) when the sea surface was not yet covered by ice. In contrast, the benthic fish *T. bernachii* confirmed its presence in a rocky inshore habitat (Williams, 1988) over the whole observation period, with a noticeable increase during the Antarctic night and the following transition period (see Figure 6). Both these species are deemed relevant and their persistence and response to climate and anthropogenic changes have been widely investigated by the marine science community (Bilyk et al., 2018; Enzor et al., 2017; Todgham & Mandic, 2020). The sea urchin *S. neumayeri* and the sea stars of genus *Odontaster* were the macrobenthos organisms that occurred most frequently during the whole observation period, as shown in Figure 6. Since these organisms are quite common along the Antarctic coasts, they have been the subject of many studies dealing with seasonal dynamics and food web architecture (Caputi et al., 2020; Dayton et al., 2019). Although other species were less frequent in the observations (e.g. the gastropod, the seaworms and the sea cucumbers), they are deemed a relevant part of the trophic structure of the benthic coastal food web (Caputi et al., 2020; Cardona et al., 2021).

In Cerrano et al. (2000), it was observed that the ingestion of the tissue of *M. acerata* by the *O. validus* and the *S. neumayeri* can lead to the total destruction of the sponge. Also the acquired images showed episodes of ingestion by the sea urchins and by the red sea stars; nevertheless, the sponge was not severely damaged by the activity of the two species within the observation period. Similarly, the sponge pumping rate and its relation

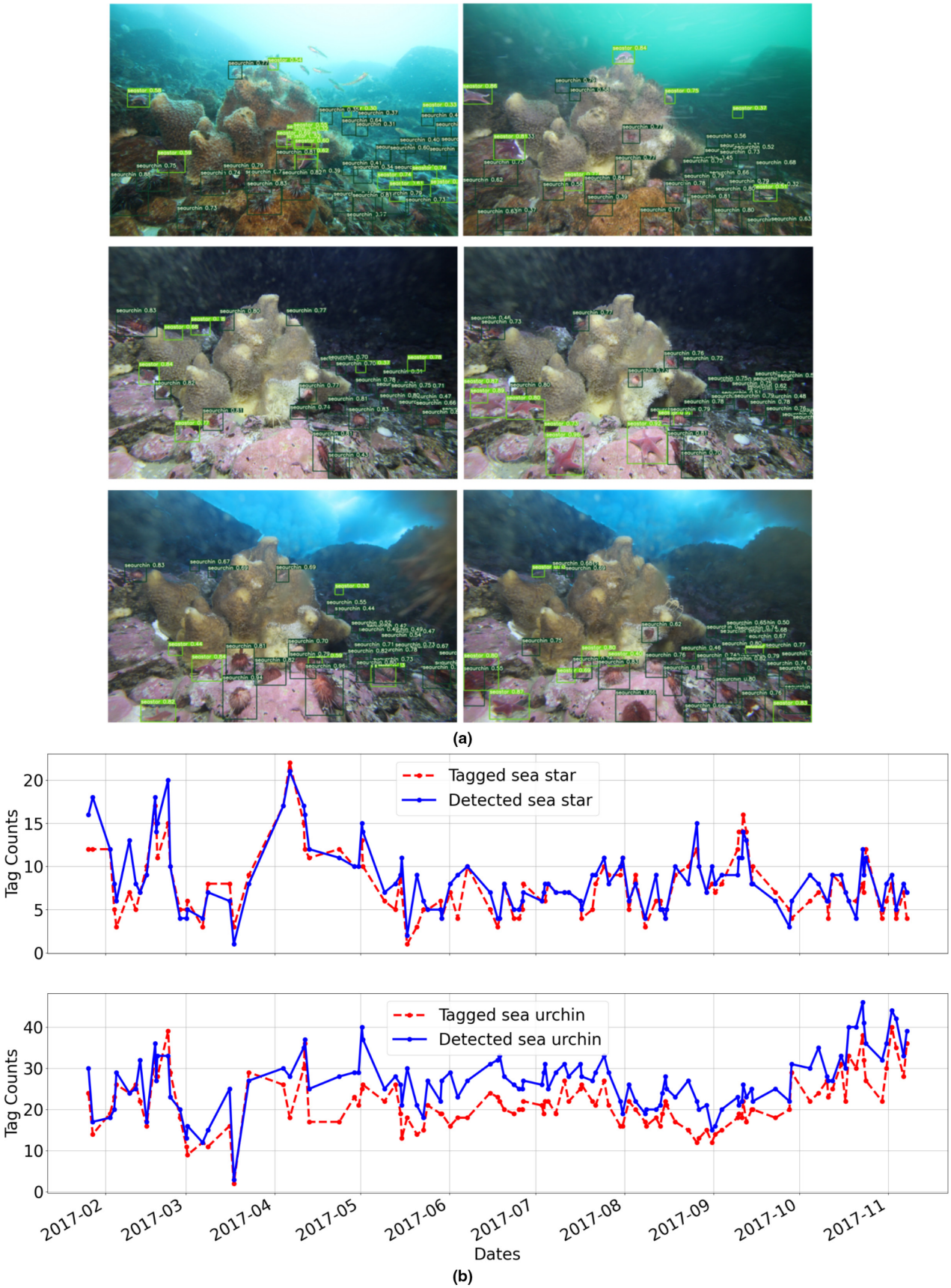


FIGURE 11 (a) Examples of YOLO classification of sea stars and sea urchins on images acquired under different conditions of underwater diffused light; (b) Comparison of organisms' tags obtained through visual inspection (dashed red line) with the YOLO automated classification (solid blue line).

to environmental factors have been rarely studied (Kowalke et al., 2001) and the long-term monitoring performed through the imaging device allowed to study interesting aspects of the sponge dynamics. In fact, while the sponge size did not vary over the observation period, the four analysed oscula showed a behaviour strongly dependent on the daylight Antarctic dynamics, as presented in Figure 10.

The success of this pilot study and the relevance of the recorded data, together with the recommendation proposed in SOOS (2017), SCAR (2021), ANTOS (2015), Convey and Peck (2019), are the steps towards the collection of continuous data on coastal bottoms in Antarctica all year around and the increase in the number of coastal stations for the monitoring of this environment. Video and image data should be collected along with the physical and chemical variables of the first 30 m of seawater, but also from offshore seawater (Cummings et al., 2018). Moreover, the acquisition of biological and oceanographic parameters should be coupled with the monitoring of Antarctic-specific features, such as, for example, the onset of freezing phenomena like the anchor ice, which may modify benthos succession and explain the scarcity or the disappearing of some key species such as bivalves and sponges in Antarctic coastal bottoms (Kim et al., 2019).

## AUTHOR'S CONTRIBUTIONS

A.P., S.M. and S.S. conceived the pilot study; S.M. and L.P.C. conceived the imaging device; A.P., S.M. and A.B. prepared and tested the imaging device for the Antarctic long-term monitoring; A.P. and S.M. participated to the XXXI Antarctic expedition where the imaging device was deployed; A.P., S.S. and F.B. visually inspected the acquired images and determined the species; S.M. conceived and developed the Computer Vision and Pattern analysis methodologies; F.B. per https://doi.org/10.5281/zenodo.641729 formed the automated detection of the organisms; all the authors wrote and reviewed the manuscript.

## ACKNOWLEDGEMENTS

The Research leading to these results has received funding from the project 'ICE-LAPSE: Analysis of Antarctic benthos dynamics by using non-destructive monitoring devices and permanent stations', PNRA 2013/AZ1.16, funded by the Italian National Antarctic Program. We are indebted to the Comando Subacquei ed Incursori (COMSUBIN) of the Italian Navy for help and assistance during the dives and to S. Cocito and C. Lombardi for their support during the test of the imaging device. We are also grateful to M. La Mesa for the determination of fish species in the captured images. This paper is also an Italian contribution to the CCAMLR CONSERVATION MEASURE 91-05 (2016) for the Ross Sea region Marine-Protected Area, specifically, addressing the priorities of Annex 91-05/C, and a contribution to the SCAR-ANTOS Expert Group (https://www.scar.org/science/antos/home/). This research activity was also partially funded by the ENDURUNS project [Horizon 2020; Grant Agreement H2020-MG-2018-2019-2020 n.824348] and the JERICO-S3 project [Horizon 2020; Grant Agreement no. 871153].

## CONFLICT OF INTEREST

The authors declare that the research was conducted in the absence of any commercial or financial relationships that could be construed as a potential conflict of interest.

## PEER REVIEW

The peer review history for this article is available at https://publons.com/publon/10.1111/2041-210X.mee313898.

## DATA AVAILABILITY STATEMENT

The image dataset and the automated image analysis code supporting this publication are available via the Zenodo repository (Marini et al., 2022a, 2022b).

## REFERENCES

Aguzzi, J., Chatzievangelou, D., Francescangeli, M., Marini, S., Bonofiglio, F., del Rio, J., & Danovaro, R. (2020). The hierarchic treatment of marine ecological information from spatial networks of benthic platforms. *Sensors*, *20*(6), 1–21. ISSN 1424-8220. https://doi.org/10.3390/s20061751

Aguzzi, J., Chatzievangelou, D., Marini, S., Fanelli, E., Danovaro, R., Flögel, S., Lebris, N., Juanes, F., De Leo, F. C., Del Rio, J., Thomsen, L., Costa, C., Riccobene, G., Tamburini, C., Lefevre, D., Gojak, C., Poulain, P.-M., Favali, P., Griffa, A., … Company, J. B. (2019). New high-tech flexible networks for the monitoring of deep-sea ecosystems. *Environmental Science & Technology*, *53*(12), 6616–6631. https://doi.org/10.1021/acs.est.9b00409

ANTOS. (2015). *Antarctic near-shore and terrestrial observing system*. Retrieved from https://www.scar.org/science/antos/home

Balog, I., Spinelli, F., Grigioni, P., Caputo, G., Napoli, G., & De Silvestri, L. (2019). Estimation of direct normal irradiance at Antarctica for concentrated solar technology. *Applied System Innovation*, *2*(3), 1–21. ISSN 2571-5577. https://doi.org/10.3390/asi2030021

Barbat, M., Rackow, T., Wesche, C., Hellmer, H., & Mata, M. (2021). Automated iceberg tracking with a machine learning approach applied to SAR imagery: A weddell sea case study. *ISPRS Journal of Photogrammetry and Remote Sensing*, *172*, 189–206. https://doi.org/10.1016/j.isprsjprs.2020.12.006

Barnes, D. (2017). Iceberg killing fields limit huge potential for benthic blue carbon in Antarctic shallows. *Global Change Biology*, *23*(7), 2649–2659. https://doi.org/10.1111/gcb.13523

Bicknell, A. W., Godley, B. J., Sheehan, E. V., Votier, S. C., & Witt, M. J. (2016). Camera technology for monitoring marine biodiversity and human impact. *Frontiers in Ecology and the Environment*, *14*(8), 424–432. https://doi.org/10.1002/fee.1322

Bilyk, K., Vargas-Chacoff, L., & Cheng, C.-H. (2018). Evolution in chronic cold: Varied loss of cellular response to heat in Antarctic notothenioid fish. *BMC Evolutionary Biology*, *18*(1), 1–16. https://doi.org/10.1186/s12862-018-1254-6

Bolinesi, F., Saggiomo, M., Ardini, F., Castagno, P., Cordone, A., Fusco, G., Rivaro, P., Saggiomo, V., & Mangoni, O. (2020). Spatial-related community structure and dynamics in phytoplankton of the Ross Sea, Antarctica. *Frontiers in Marine Science*, *7*, 1092. ISSN 2296-7745. https://doi.org/10.3389/fmars.2020.574963

Brasier, M., Constable, A., Melbourne-Thomas, J., Trebilco, R., Griffiths, H., Van de Putte, A., & Sumner, M. (2019). Observations and models to support the first Marine Ecosystem Assessment for the Southern Ocean (MEASO). *Journal of Marine Systems*, *197*, 103182. ISSN 0924-7963. https://doi.org/10.1016/j.jmarsys.2019.05.008

Caputi, S. S., Careddu, G., Calizza, E., Fiorentino, F., Maccapan, D., Rossi, L., & Costantini, M. L. (2020). Seasonal food web dynamics in the Antarctic benthos of Tethys Bay (Ross Sea): Implications for biodiversity persistence under different seasonal sea-ice coverage. *Frontiers in Marine Science*, *7*, 1046. ISSN 2296-7745. https://doi.org/10.3389/fmars.2020.594454

Cardona, L., Lloret-Lloret, E., Moles, J., & Avila, C. (2021). Latitudinal changes in the trophic structure of benthic coastal food webs along the Antarctic Peninsula. *Marine Environmental Research*, *167*, 105290. ISSN 0141-1136. https://doi.org/10.1016/j.marenvres.2021.105290

Cecchetto, M., Di Cesare, A., Eckert, E., Fassio, G., Fontaneto, D., Moro, I., Oliverio, M., Sciuto, K., Tassistro, G., Vezzulli, L., & Schiaparelli, S. (2021). Antarctic coastal nanoplankton dynamics revealed by metabarcoding of desalination plant filters: Detection of short-term events and implications for routine monitoring. *Science of The Total Environment*, *757*, 143809. ISSN 0048–9697. https://doi.org/10.1016/j.scitotenv.2020.143809

Cerrano, C., Bavestrello, G., Calcinai, B., Cattaneo-Vietti, R., & Sarà, A. (2000). Asteroids eating sponges from Tethys Bay, east Antarctica. *Antarctic Science*, *12*(4), 425–426. https://doi.org/10.1017/s0954102000000050x

Clark, M., Nieva, L. V., Hoffman, J., Davies, A., Trivedi, U., Turner, F., Ashton, G., & Peck, L. (2019). Lack of long-term acclimation in Antarctic encrusting species suggests vulnerability to warming. *Nature Communications*, *10*(1), 1–10. https://doi.org/10.1038/s41467-019-11348-w

COCO. (2021). *Common objects in context*. Retrieved from https://cocodataset.org/

Convey, P., & Peck, L. S. (2019). Antarctic environmental change and biological responses. *Science Advances*, *5*(11), 1–16. https://doi.org/10.1126/sciadv.aaz0888

Corgnati, L., Marini, S., Mazzei, L., Ottaviani, E., Aliani, S., Conversi, A., & Griffa, A. (2016). Looking inside the ocean: Toward an autonomous imaging system for monitoring gelatinous zooplankton. *Sensors*, *16*(12), 2124. ISSN 1424-8220. https://doi.org/10.3390/s16122124

CR2. (2021). *The Canon RAW (CRW) File Format*. Retrieved from https://exiftool.org

Cummings, V. J., Hewitt, J. E., Thrush, S. F., Marriott, P. M., Halliday, N. J., & Norkko, A. (2018). Linking ross sea coastal benthic communities to environmental conditions: Documenting baselines in a spatially variable and changing world. *Frontiers in Marine Science*, *5*, 232. ISSN 2296-7745. https://doi.org/10.3389/fmars.2018.00232

Dañobeitia, J. J., Pouliquen, S., Johannessen, T., Basset, A., Cannat, M., Pfeil, B. G., Fredella, M. I., Materia, P., Gourcuff, C., Magnifico, G., Delory, E., del Rio Fernandez, J., Rodero, I., Beranzoli, L., Nardello, I., Iudicone, D., Carval, T., Aranda, J. M. G., Petihakis, G., … Favali, P. (2020). Toward a comprehensive and integrated strategy of the European marine research infrastructures for ocean observations. *Frontiers in Marine Science*, *7*, 180. ISSN 2296-7745. https://doi.org/10.3389/fmars.2020.00180

Dark Channel Prior Dehazing. (2015). *Python implementation of single image haze removal using dark channel prior*. Retrieved from https://github.com/joyeecheung/dark-channel-prior-dehazing

Dayton, P. K., Jarrell, S. C., Kim, S., Ed Parnell, P., Thrush, S. F., Hammerstrom, K., & Leichter, J. J. (2019). Benthic responses to an Antarctic regime shift: Food particle size and recruitment biology. *Ecological Applications*, *29*(1), e01823. https://doi.org/10.1002/eap.1823

Dougherty, G. (2013). Pattern recognition and classification. *An introduction*. Springer. ISBN 978-1-4614-5322-2.

Enzor, L. A., Hunter, E. M., & Place, S. P. (2017). The effects of elevated temperature and ocean acidification on the metabolic pathways of notothenioid fish. *Conservation Physiology*, *5*(1), cox019. ISSN 2051-1434. https://doi.org/10.1093/conphys/cox019

European Marine Board. (2020). *Working Group on Big Data in Marine Science*. Retrieved from https://www.marineboard.eu/publications/big-data-marine-science

Fawcett, T. (2006). An introduction to roc analysis. *Pattern Recognition Letters*, *27*(8), 861–874. ISSN 0167-8655. https://doi.org/10.1016/j.patrec.2005.10.010 ROC Analysis in Pattern Recognition.

Gutt, J., Arndt, J., Kraan, C., Dorschel, B., Schröder, M., Bracher, A., & Piepenburg, D. (2019). Benthic communities and their drivers: A spatial analysis off the Antarctic Peninsula. *Limnology and Oceanography*, *64*(6), 2341–2357. https://doi.org/10.1002/lno.11187

Harrison, D., De Leo, F., Gallin, W., Mir, F., Marini, S., & Leys, S. (2021). Machine learning applications of convolutional neural networks and unet architecture to predict and classify demosponge behavior. *Water (Switzerland)*, *13*(18), 1–17. https://doi.org/10.3390/w13182512

Jahanbakht, M., Xiang, W., Hanzo, L., & Azghadi, M. R. (2021). Internet of underwater things and big marine data analytics – A comprehensive survey. *IEEE Communications Surveys Tutorials*, *23*(2), 904–956. https://doi.org/10.1109/COMST.2021.3053118

Kim, M., Yang, E., Kim, H., Kim, D., Kim, T.-W., Sul La, H., Lee, S., & Hwang, J. (2019). Collection of large benthic invertebrates in sediment traps in the Amundsen sea, Antarctica. *Biogeosciences*, *16*(13), 2683–2691. https://doi.org/10.5194/bg-16-2683-2019

Kim, S. L., Thurber, A., Hammerstrom, K., & Conlan, K. (2007). Seastar response to organic enrichment in an oligotrophic polar habitat. *Journal of Experimental Marine Biology and Ecology*, *346*(1), 66–75. ISSN 0022-0981. https://doi.org/10.1016/j.jembe.2007.03.004

Kohavi, R. (1995). A study of cross-validation and bootstrap for accuracy estimation and model selection. In *Proceedings of the 14th International Joint Conference on Artificial Intelligence - Volume 2*, IJCAI'95 (pp. 1137–1143). Morgan Kaufmann Publishers Inc. ISBN 1-55860-363-8.

Kowalke, J., Tatián, M., Sahade, R., & Arntz, W. (2001). Production and respiration of Antarctic ascidians. *Polar Biology*, *24*(9), 663–669. https://doi.org/10.1007/s003000100266

LabelImg. (2021). *A graphical image annotation tool*. Retrieved from https://github.com/tzutalin/labelImg

Langenkämper, D., van Kevelaer, R., Purser, A., & Nattkemper, T. W. (2020). Gear-induced concept drift in marine images and its effect on deep learning classification. *Frontiers in Marine Science*, *7*, 506. ISSN 2296-7745. https://doi.org/10.3389/fmars.2020.00506

Langenkämper, D., Zurowietz, M., Schoening, T., & Nattkemper, T. W. (2017). Biigle 2.0 - Browsing and annotating large marine image collections. *Frontiers in Marine Science*, *4*, 1–10. https://doi.org/10.3389/fmars.2017.00083

Lopez-Vazquez, V., Lopez-Guede, J. M., Marini, S., Fanelli, E., Johnsen, E., & Aguzzi, J. (2020). Video image enhancement and machine learning pipeline for underwater animal detection and classification at cabled observatories. *Sensors*, *20*(3), 1–25. ISSN 1424-8220. https://doi.org/10.3390/s20030726

MacLeod, N., Benfield, M., & Culverhouse, P. (2010). Time to automate identification. *Nature*, *467*(7312), 154–155. ISSN 1476-4687. https://doi.org/10.1038/467154a

Magic Lantern. (2021). Retrieved from https://magiclantern.fm

Malde, K., Handegard, N. O., Eikvil, L., & Salberg, A.-B. (2019). Machine intelligence and the data-driven future of marine science. *ICES Journal of Marine Science*, *77*(4), 1274–1285. ISSN 1054-3139. https://doi.org/10.1093/icesjms/fsz057

Malyarenko, A., Wells, A., Langhorne, P., Robinson, N., Williams, M., & Nicholls, K. (2020). A synthesis of thermodynamic ablation at ice–ocean interfaces from theory, observations and models. *Ocean Modelling*, *154*, 1–25. https://doi.org/10.1016/j.ocemod.2020.101692

Marini, S., Bonofilgio, F., Corgnati, L. P., Bordone, A., Schiaparelli, S., & Peirano, A. (2022a). Image dataset supporting the publication

"Long-term automated visual monitoring of Antarctic benthic fauna". https://doi.org/10.5281/zenodo.6418163

Marini, S., Bonofilgio, F., Corgnati, L. P., Bordone, A., Schiaparelli, S., & Peirano, A. (2022b). Image analysis tools supporting the publication "Long-term automated visual monitoring of Antarctic benthic fauna". https://doi.org/10.5281/zenodo.6417294

Marini, S., Corgnati, L., Mantovani, C., Bastianini, M., Ottaviani, E., Fanelli, E., Aguzzi, J., Griffa, A., & Poulain, P.-M. (2018). Automated estimate of fish abundance through the autonomous imaging device guard. *Measurement*, *126*, 72–75. ISSN 0263-2241. https://doi.org/10.1016/j.measurement.2018.05.035

Marini, S., Fanelli, E., Sbragaglia, V., Azzurro, E., Del Rio Fernandez, J., & Aguzzi, J. (2018). Tracking fish abundance by underwater image recognition. *Scientific Reports*, *8*(1), 13748. ISSN 2045-2322. https://doi.org/10.1038/s41598-018-32089-8

Marini, S., Griffa, A., Aliani, S., Conversi, A., Shroeder, K., & Borghini, M. (2013). EP2863257 (A1) - Underwater images acquisition and processing system. Retrieved from https://data.epo.org/gpi/EP2863257B1

Moeslund, T. B. (2012). *Introduction to video and image processing*. Springer. ISBN 978-1-4471-2503-7. https://doi.org/10.1007/978-1-4471-2503-7

Möller, T., & Nattkemper, T. W. (2021). Almi – A generic active learning system for computational object classification in marine observation images. *Sensors*, *21*(4), 1–16. ISSN 1424-8220. https://doi.org/10.3390/s21041134

Möller, T., Nilssen, I., & Nattkemper, T. (2019). Tracking sponge size and behaviour with fixed underwater observatories. *Lecture Notes in Computer Science (including subseries Lecture Notes in Artificial Intelligence and Lecture Notes in Bioinformatics)*, 11188 LNCS:45-54. https://doi.org/10.1007/978-3-030-05792-3_5

Moran, K., Boutin, B., Juniper, S., Pirenne, B., & Round, A. (2019). A multi-use and multi-stakeholder ocean observing platform system. https://doi.org/10.23919/OCEANS40490.2019.8962711

OEngineering. (2021). *OEngineering s.r.l. - GUARD-1, Underwater Autonomous Smart Camera*. Retrieved from https://www.oengineering.eu//GUARD-1/

OpenCV. (2021). *Open source computer vision library*. Retrieved from https://opencv.org/

Osterloff, J., Nilssen, I., Järnegren, J., Van Engeland, T., Buhl-Mortensen, P., & Nattkemper, T. (2019). Computer vision enables short- and long-term analysis of lophelia pertusa polyp behaviour and colour from an underwater observatory. *Scientific Reports*, *9*(1), 1–12. https://doi.org/10.1038/s41598-019-41275-1

Painting, S., Collingridge, K., Durand, D., Grémare, A., Créach, V., & Bernard, G. (2020). Marine monitoring in europe: Is it adequate to address environmental threats and pressures? *Ocean Science*, *16*(1), 235–252. https://doi.org/10.5194/os-16-235-2020

Peck, L. S. (2018). Antarctic marine biodiversity: Adaptations, environments and responses to change. In S. Hawkins, A. Evans, A. Dale, L. Firth, I. Smith, & D. Hughes (Eds.), *Oceanography and marine biology: An annual review, vol 56, oceanography and marine biology* (pp. 105–236). CRC Press-Taylor & Francis Group. ISBN 978-0-429-45445-5; 978-1-138-31862-5.

Peirano, A., Bordone, A., Marini, S., Piazza, P., & Schiaparelli, S. (2016). A simple time-lapse apparatus for monitoring macrozoobenthos activity in Antarctica. *Antarctic Science*, *28*(6), 473–474. https://doi.org/10.1017/S0954102016000377

Peng, Y., Cao, K., & Cosman, P. C. (2018). Generalization of the dark channel prior for single image restoration. *IEEE Transactions on Image Processing*, *27*(6), 2856–2868. https://doi.org/10.1109/TIP.2018.2813092

Piazza, P., Cummings, V., Guzzi, A., Hawes, I., Lohrer, A., Marini, S., Marriott, P., Menna, F., Nocerino, E., Peirano, A., Kim, S., & Schiaparelli, S. (2019). Underwater photogrammetry in Antarctica: Long-term observations in benthic ecosystems and legacy data rescue. *Polar Biology*, *42*(6), 1061–1079. https://doi.org/10.1007/s00300-019-02480-w

Piazza, P., Cummings, V., Lohrer, D., Marini, S., Marriott, P., Menna, F., Nocerino, E., Peirano, A., & Schiaparelli, S. (2018). Divers-operated underwater photogrammetry: Applications in the study of Antarctic benthos. *International Archives of the Photogrammetry, Remote Sensing and Spatial Information Sciences*, *42*, 885–892. https://doi.org/10.5194/isprs-archives-XLII-2-885-2018

Piazza, P., Gattone, S., Guzzi, A., & Schiaparelli, S. (2020). Towards a robust baseline for long-term monitoring of Antarctic coastal benthos. *Hydrobiologia*, *847*(7), 1753–1771. https://doi.org/10.1007/s10750-020-04177-2

Pineda-Metz, S., Gerdes, D., & Richter, C. (2020). Benthic fauna declined on a whitening Antarctic continental shelf. *Nature Communications*, *11*(1), 1–7. https://doi.org/10.1038/s41467-020-16093-z

Rajesh, K., & Lalitha Bhaskari, D. (2020). Automatic image annotation: A review of recent advances and literature. *Smart Innovation, Systems and Technologies*, *160*, 271–281. https://doi.org/10.1007/978-981-32-9690-9_27

Ramesh, K., & Soni, V. (2018). Perspectives of Antarctic weather monitoring and research efforts. *Polar Science*, *18*, 183–188. https://doi.org/10.1016/j.polar.2018.04.005

Raspberry Pi Foundation. (2021). Retrieved from https://www.raspberrypi.org/

Redmon, J., Divvala, S., Girshick, R., & Farhadi, A. (2016). You only look once: Unified, real-time object detection. In *2016 IEEE Conference on Computer Vision and Pattern Recognition (CVPR)*, pp. 779–788. ISBN: 978-1-4673-8851-1. https://doi.org/10.1109/CVPR.2016.91

Rignot, E., Mouginot, J., Scheuchl, B., Van Den Broeke, M., Van Wessem, M., & Morlighem, M. (2019). Four decades of Antarctic ice sheet mass balance from 1979–2017. *Proceedings of the National Academy of Sciences of the United States of America*, *116*(4), 1095–1103. https://doi.org/10.1073/pnas.1812883116

Rogers, A., Frinault, B., Barnes, D., Bindoff, N., Downie, R., Ducklow, H., Friedlaender, A., Hart, T., Hill, S., Hofmann, E., Linse, K., McMahon, C., Murphy, E., Pakhomov, E., Reygondeau, G., Staniland, I., Wolf-Gladrow, D., & Wright, R. (2020). Antarctic futures: An assessment of climate-driven changes in ecosystem structure, function, and service provisioning in the southern ocean. *Annual Review of Marine Science*, *12*(1), 87–120. https://doi.org/10.1146/annurev-marine-010419-011028

Rountree, R., Aguzzi, J., Marini, S., Fanelli, E., de Leo, F., Rio, J., & Juanes, F. (2020). Towards an optimal design for ecosystem-level ocean observatories. *Oceanography and Marine Biology*, *58*, 79–105. https://doi.org/10.1201/9780429351495-2

SCAR. (2021). Scientific Committee on Antarctic Research. Retrieved from https://www.scar.org

Schoening, T., Osterloff, J., & Nattkemper, T. W. (2016). Recomia—recommendations for marine image annotation: Lessons learned and future directions. *Frontiers in Marine Science*, *3*, 1–11. ISSN 2296-7745. https://doi.org/10.3389/fmars.2016.00059

Shi, W., Cao, J., Zhang, Q., Li, Y., & Xu, L. (2016). Edge computing: Vision and challenges. *IEEE Internet of Things Journal*, *3*(5), 637–646. https://doi.org/10.1109/JIOT.2016.2579198

Shi, Z., Zhu, M., Guo, B., Zhao, M., & Zhang, C. (2018). Nighttime low illumination image enhancement with single image using bright/dark channel prior. *EURASIP Journal on Image and Video Processing*, *1*, 2018. https://doi.org/10.1186/s13640-018-0251-4

SOOS. (2017). *Southern ocean observing system – Report on the 2017 Ross sea working group meeting*. Retrieved from http://www.soos.aq

Srivastava, S., Divekar, A., Anilkumar, C., Naik, I., Kulkarni, V., & Pattabiraman, V. (2021). Comparative analysis of deep learning image detection algorithms. *Journal of Big Data*, *8*(1), 1–27. https://doi.org/10.1186/s40537-021-00434-w

Todgham, A. E., & Mandic, M. (2020). Understanding the metabolic capacity of Antarctic fishes to acclimate to future ocean conditions. *Integrative and Comparative Biology*, *60*(6), 1425–1437. ISSN 1540-7063. https://doi.org/10.1093/icb/icaa121

Vacchi, M., La Mesa, M., & Greco, S. (2000). *The Coastal Fish Fauna of Terra Nova Bay, Ross Sea, Antarctica* (pp. 457–468). Springer Berlin Heidelberg. https://doi.org/10.1007/978-3-642-59607-0_32

van Leeuwe, M. A., Webb, A. L., Venables, H. J., Visser, R. J., Meredith, M. P., Elzenga, J. T. M., & Stefels, J. (2020). Annual patterns in phytoplankton phenology in Antarctic coastal waters explained by environmental drivers. *Limnology and Oceanography*, *65*(7), 1651–1668. https://doi.org/10.1002/lno.11477

Wan Hussin, W. M. R., Husin, A., Syed Mahdzar, S. F., & Mohd Nadzir, M. S. (2019). Preliminary investigation on the structural, taxonomic and functional diversities of benthic communities at different areas in the west Antarctic Peninsula. *Polar Science*, *20*, 100–106. ISSN 1873-9652. https://doi.org/10.1016/j.polar.2019.01.002

Watters, G., Hinke, J., & Reiss, C. (2020). Long-term observations from Antarctica demonstrate that mismatched scales of fisheries management and predator-prey interaction lead to erroneous conclusions about precaution. *Scientific Reports*, *10*(1), 1–9. https://doi.org/10.1038/s41598-020-59223-9

Williams, R. (1988). The inshore marine fishes of the vestfold hills region, Antarctica. *Hydrobiologia*, *165*, 161–167. ISSN 0018-8158. https://doi.org/10.1007/BF00025583

YOLO V5. (2021). Retrieved from https://github.com/ultralytics/yolov5

Zampoukas, N., Palialexis, A., Duffek, A., Graveland, J., Giorgi, G., Hagebro, C., Hanke, G., Korpinen, S., Tasker, M., Tornero, V., Abaza, V., Battaglia, P., Caparis, M., Dekeling, R., Frias Vega, M., Haarich, M., Katsanevakis, S., Klein, H., Krzyminski, W., … Zevenboom, W. (2014). Technical guidance on monitoring for the marine strategy framework directive. Technical report, European Commission, Report EUR 26499, 01.

Zhu, L., Xie, Z., Liu, L., Tao, B., & Tao, W. (2021). IoU-uniform R-CNN: Breaking through the limitations of RPN. *Pattern Recognition*, *112*, 107816. ISSN 0031-3203. https://doi.org/10.1016/j.patcog.2021.107816

Zhuang, F., Qi, Z., Duan, K., Xi, D., Zhu, Y., Zhu, H., Xiong, H., & He, Q. (2021). A comprehensive survey on transfer learning. *Proceedings of the IEEE*, *109*(1), 43–76. https://doi.org/10.1109/JPROC.2020.3004555

Zuazo, A., Grinyó, J., López-Vàzquez, V., Rodríguez, E., Costa, C., Ortenzi, L., Flögel, S., Valencia, J., Marini, S., Zhang, G., Wehde, H., & Aguzzi, J. (2020). An automated pipeline for image processing and data treatment to track activity rhythms of paragorgia arborea in relation to hydrographic conditions. *Sensors*, *20*(21), 1–23. ISSN 1424-8220. https://doi.org/10.3390/s20216281

Zurowietz, M., Langenkämper, D., Hosking, B., Ruhl, H., & Nattkemper, T. (2018). Maia – A machine learning assisted image annotation method for environmental monitoring and exploration. *PLoS ONE*, *13*(11), 1–18. https://doi.org/10.1371/journal.pone.0207498

## SUPPORTING INFORMATION

Additional supporting information may be found in the online version of the article at the publisher's website.

**How to cite this article:** Marini, S., Bonofiglio, F., Corgnati, L. P., Bordone, A., Schiaparelli, S., & Peirano, A. (2022). Long-term automated visual monitoring of Antarctic benthic fauna. *Methods in Ecology and Evolution*, *13*, 1746–1764. https://doi.org/10.1111/2041-210X.13898